Asymmetrizing an icosahedral virus capsid by hierarchical assembly of subunits with designed asymmetry

Zhongchao Zhao
Department of Molecular and Cellular Biochemistry, Indiana University, Bloomington, Indiana
https://orcid.org/0000-0002-3736-6677
Joseph Wang
Penn State Milton S. Hershey Medical Center
Mi Zhang
Indiana University Bloomington
Nicholas Lyktey
Indiana University Bloomington
Martin Jarrold
Indiana University
Stephen Jacobson
Indiana University Bloomington https://orcid.org/0000-0003-2415-041X
Adam Zlotnick (azlotnic@iu.edu)
Indiana University Bloomington

Article

Keywords: Asymmetrizing, icosahedral virus capsid, designed asymmetry

Posted Date: July 17th, 2020

DOI: https://doi.org/10.21203/rs.3.rs-36394/v1

Version of Record: A version of this preprint was published at Nature Communications on January 26th, 2021. See the published version at https://doi.org/10.1038/s41467-020-20862-1.

Abstract

Symmetrical protein complexes are ubiquitous in natural biological systems. Many have been reengineered *in vitro* for chemical and medical applications. Symmetrical viral capsids and their assembly are frequent platforms for these investigations. Lacking a means to create asymmetric capsids may limit broader applications. Here, starting with the homodimeric Hepatitis B Virus capsid protein, we developed a heterodimer, designed a hierarchical assembly pathway, and produced asymmetric capsids. We showed that the heterodimers assemble into hexamers, and such preformed hexamers can nucleate co-assembly, leading to “Janus” capsids with two discrete patches. We removed the hexamer patches specifically and observed asymmetric holey capsids by cryo-EM reconstruction. The resulting holes can be refilled with new engineered dimers. This programmed assembly pathway provides windows for specific engineering and modification inside and outside of the capsid. This strategy can also be generalized to other capsid assembly systems.

Introduction

Symmetrical supramolecular protein complexes are ubiquitous in natural biological systems to compartmentalize and execute complex functions[1-5]. Many groups have attempted to take advantage of natural systems to develop nanotechnologies, such as drug delivery, energy transport and information storage[6-17]. Symmetrical viral capsids and their assembly are frequent platforms for these investigations[18-22]. Many viral capsids have icosahedral symmetry and are assembled from a single symmetrical building block[23-26]. The simplicity of viral capsids provides many advantages. However, symmetrical subunits offer little or no opportunity to control the reaction and to incorporate specific asymmetric features. This shortcoming may limit development of applications that need conditional stops for information insertion and cargo loading. Engineering a controlled assembly pathway with designed pauses is a strategy to overcome this drawback and support hierarchical assembly of a capsid.

Although capsid assembly has nucleation and elongation phases, there are no discrete stopping points for manipulation and modification of specific intermediates[27-29]. Here, we used Hepatitis B Virus (HBV) capsid assembly as a model system and demonstrated an effective approach to break the spontaneous assembly into addressable steps[28,30,31]. HBV dimers interact when the end of the “contact helix” of one subunit fits into a groove formed by the contact helix of an adjacent subunit (note the hexamer in Fig. 1). Of course, a dimer has contact helices at either end[23,32,33]. In concept, both monomers can be engineered differently, leading to a heterodimer for which each monomer can assemble in response to a specific condition. One extreme example would be a heterodimer with an assembly-active monomer and an assembly-incompetent monomer[34-36]. We designed such a heterodimer and have used it to generate small complexes that, in turn, can nucleate assembly of a capsid. The co-assembled capsid has two discrete and addressable patches[37-39], a heterodimer patch and a homodimer patch, analogous to a Janus particle[40,41]. The chemically distinct nature of the two patches give us the ability to control further

modification, disassembly, and reassembly. In this paper, we describe this platform and some basic manipulations of controlled assembly.

Materials And Methods

A complete materials and methods section is available in supplementary information.

Design and expression of pET11a-Cp149$_{His}$Cp149$_{Y132A}$. Design of bicistronic pET11a-Cp149$_{His}$Cp149$_{Y132A}$ is described in Supplementary Fig. 1. Cp149$_{His}$Cp149$_{Y132A}$, was purified based on the protocol for Cp149$_{Y132A}$ with modifications[36], Cp149 and Cp150 homodimers were purified as described previously[42].

Assembly of hexamer, co-assembly, disassembly, and refilling. All buffers include 50 mM HEPES pH 7.5. To assemble hexamers, a 1:10 ratio of Cp149$_{His}$Cp149$_{Y132A}$ to $NiCl_2$ in 50 mM HEPES was incubated at 23°C for 1 h. To use hexamers as nuclei for co-assembly, 4:1 Cp150 dimer to Cp149$_{His}$Cp149$_{Y132A}$ was mixed with the pre-assembled hexamers, leading to a 4:1:10 ratio of Cp150 dimer : Cp149$_{His}$Cp149$_{Y132A}$: $NiCl_2$, and incubated for 10 min at 23°C. For co-assembly, a 300 mM NaCl buffer was used. To remove hexamers from co-assembled capsids and create holey capsids, purified capsids were mixed with 3 M urea and 100 uM EDTA and incubated at 23°C for 24 h. Holey capsids were purified with an Amicon Ultra-Cel with 100 kDa cutoff to remove Cp149$_{His}$Cp149$_{Y132A}$ subunits and washed 4 times with 150 mM NaCl. All the analytical size exclusion chromatography was carried out with a Superose 6 10/300 GL column (GE Healthcare) equilibrated in 50 mM HEPES (pH 7.5) for dimer characterization, with 150 mM NaCl for holey capsids, and with 300 mM NaCl for hexamer and complete capsids.

Charge Detection Mass Spectrometry (CDMS). To test hexamer formation with CDMS, buffer was replaced by volatile 20 mM ammonium acetate for protein and $NiCl_2$. The homebuilt CDMS instrument has been described previously[43].

Resistive-Pulse Sensing (RPS). Resistive-pulse sensing is a single molecule detection method which permits real-time and label-free characterization of individual HBV capsids[44,45]. Resistive-pulse measurements were conducted on the initially assembled capsids, holey capsids, and refilled capsids. Capsid samples were diluted to dimer concentrations of ≤ 0.1 μM in 1 M NaCl and loaded onto a nanofluidic device with 4 pores in series. To improve the signal-to-noise ratio, samples were cycled back and forth through the device n times (i.e., ping-pong)[46]. T = 3 and T = 4 Cp150 capsids were used as standards.

Results And Discussion

Design of a new pathway for asymmetric capsid assembly. To create an asymmetric assembly pathway with asymmetric capsids requires a means to initiate assembly with a specific complex and a means of halting and possibly restarting assembly at a specific juncture. As an example, we designed an asymmetric assembly pathway from asymmetric subunits to asymmetric holey capsids, and eventually to asymmetric T=4 capsids (Fig. 1). With this designed pathway, we created stages in the reaction, which yield opportunities for modifications and engineering.

To achieve asymmetric assembly, we modified the 149-residue HBV capsid protein assembly domain, Cp149. We created a heterodimeric subunit, $Cp149_{His}Cp149_{Y132A}$ (Fig. 2a) that possesses functionalities on each monomer, one encoding a programable assembly function and the other encoding a conditional stop. The assembly active monomer can assemble in response to ionic strength, like wildtype dimer, and is also sensitive to Ni^{2+} due to the addition of a His-Tag[47]. The conditional stop monomer carries the assembly-incompetent mutation Y132A, which inhibits assembly due to loss of hydrophobic surface for proper subunit interactions; however, it can still co-assemble with wildtype dimers into labile capsids[34-36].

In our engineered assembly path (Fig. 1), the asymmetric heterodimers assemble in response to Ni^{2+} but will stop after forming an initial complex, a hexamer in this diagram, due to the influence of Y132A. Hexamers then can be used as nuclei to co-assemble with a second species of dimer, in response to high ionic strength. The resulting hybrid capsids have two distinct patches, the hexamer nucleus and the homodimer component. To further manipulate the structure, we differentially stabilize the patches, which can be accomplished by using a homodimer that can spontaneously form crosslinks[48,49]. Here, we used Cp150 homodimers. As a Cp149 variant, Cp150 incorporates a C-terminal cysteine that clusters at fivefold and quasi-sixfold vertices resulting in disulfide crosslinks[32,48,49]. Crosslinked regions in hybrid capsids are stable under low ionic strength and urea treatment. Because the heterodimer lacks cysteine 150 and fails to crosslink, heterodimer patches can be removed specifically, leaving crosslinked asymmetric holey capsids. Such holey capsids then can be further modified, and/or the hole can be refilled with new subunits to generate symmetric or asymmetric, un-holey T=4 complete capsids.

In summary, we have a series of essentially orthogonal reactions that allow us to engineer novel features into each step of a hierarchical assembly: (i) nucleate, (ii) elongate to create a “body”, (iii) crosslink capsid body, (iv) remove nucleus, and (v) refill the hole.

Purification and characterization of heterodimer $Cp149_{His}Cp149_{Y132A}$. To generate the asymmetric heterodimer $Cp149_{His}Cp149_{Y132A}$, we designed a bicistronic expression plasmid (Supplementary Fig. 1).

This approach has been used to split a single monomer into two segments, called SplitCore, which can still dimerize, to incorporate oversized proteins for vaccine development[50]. The bicistronic plasmid carries a single promoter and two genes for each monomer, $Cp149_{His}$ and $Cp149_{Y132A}$. Each gene has its own ribosome binding site (RBS). Following *E.coli* expression, $Cp149_{His}Cp149_{Y132A}$ was purified as a dimer and characterized. The yield of purified protein was ~50 mg per liter of LB broth. $Cp149_{His}Cp149_{Y132A}$ eluted as a single peak on size-exclusion chromatography (SEC) at the same position as homodimer Cp149 (Fig. 2b). $Cp149_{His}Cp149_{Y132A}$ was resolved on SDS-PAGE, showing approximately equal amounts of two bands corresponding to the Y132A and the His-tag monomers (Fig. 2b, inset). Native mass spectrometry (MS) of heterodimer $Cp149_{His}Cp149_{Y132A}$ showed three peaks corresponding to $Cp149_{His}$ monomer, $Cp149_{Y132A}$ monomer, and heterodimer comprised of $Cp149_{His}$ and $Cp149_{Y132A}$ (Fig. 2c). There was no evidence of either $Cp149_{His}$ or $Cp149_{Y132A}$ homodimers in the MS analysis.

Efficient expression of highly purified heterodimer is an important step towards asymmetric assembly in this study. An asymmetric dimer may also be useful for vaccine development and other applications[50-53]. The splitcore system allowed incorporation of large inserts but still generated a symmetric dimer[50]. An HBV tandem dimer comprised of two monomers linked by a short peptide was developed[54,55]. However, in our hands we observed the tandem dimer had low yield and generated many aggregates that suggested that the linkage between monomers may have led to misfolding. The bicistronic heterodimer expression system retained monomer integrity, while still providing the opportunity to modify each monomer independently. We believe that our system has potential for larger changes, e.g., peptide and protein insertion for antigen presentation.

Heterodimer $Cp149_{His}Cp149_{Y132A}$ assembles hexamer. Because heterodimer carries the assembly-incompetent mutation Y132A[34-36], we first compared the assembly induced by high ionic strength (300 mM NaCl) of $Cp149_{His}Cp149_{Y132A}$ and wild-type homodimer Cp149. As anticipated, $Cp149_{His}Cp149_{Y132A}$ failed to assemble capsids, and no stable intermediates were isolated under conditions where Cp149 assembled readily (Supplementary Fig. 2).

We then tested assembly of $Cp149_{His}Cp149_{Y132A}$ in response to Ni^{2+} at low ionic strength, taking advantage of the His-tag without involving ionic strength-driven assembly (Fig. 3). We typically used 10 μM heterodimer and 100 μM $NiCl_2$ for these reactions. We observed by SEC that $Cp149_{His}Cp149_{Y132A}$ assembles into heterogeneous complexes that are larger than dimers. Using charge detection mass spectrometry (CDMS), a single molecule technique capable of resolving the masses of complex mixtures[56], we found that major species were hexamers, dimers of dimers, and free dimers (Fig. 3b). The larger complexes were isolated by SEC and visualized by negative-stain electron microscopy (EM). Particles from micrographs were semi-manually selected and subjected to 2D classification, resulting in top and side views of hexamers and double hexamers (Fig. 3c). Due to the limited number of particles, a density map of double hexamer was not reconstructed. The top 8 classes were selected for reconstructing a 3D density map that reached 17 Å resolution. The resulting density map confirmed

assembly of capsid-like hexamers by $Cp149_{His}Cp149_{Y132A}$ (Fig. 3d). A hexamer molecular model, isolated from an HBV capsid[57], fit well into the density. Thus, unlike symmetric homodimers, which assemble into capsids with very low concentrations of intermediates, asymmetric $Cp149_{His}Cp149_{Y132A}$ heterodimers assemble to hexamers or double hexamers and then assembly stops. Successful hexamer and double hexamer formation also suggest that species with different sizes can be produced with other mutations.

$Cp149_{His}Cp149_{Y132A}$ hexamers co-assemble with homodimers. While the Y132A mutant is assembly incompetent on its own, it can co-assemble with Cp149[34-36]. We reasoned that the hexameric complex that assembled in response to Ni^{2+} could nucleate further assembly, because each incoming dimer will make two contacts to the nucleating hexamer, only one of which was compromised by the Y132A mutation. Thus, the Y132A may weaken the initial steps of assembly but will not prevent it. To test this hypothesis, we co-assembled preformed hexamers with homodimers, in effect making a Janus particle with a nucleus patch and a homodimer patch[40,41]. As mentioned above, we chose Cp150 homodimers that can crosslink for co-assembly reaction to ensure that the homodimer component would be sturdy enough to allow subsequent removal of the heterodimer hexamers.

We observed although heterodimer polymerization stops at hexamers, hexamers can nucleate ionic strength-driven (300 mM NaCl) assembly of Cp150 homodimers, forming hybrid capsids; adding heterodimer hexamers to an assembly reaction promoted assembly and decreased the apparent pseudo-critical concentration of assembly (Fig. 4a). As a control, we observed that Ni^{2+} at a concentration of 100 μM had no measurable effect on Cp150 assembly (Supplementary Fig. 3). Free $Cp149_{His}Cp149_{Y132A}$ heterodimers can co-assemble with Cp150 to form morphologically normal capsids but there is no evidence that the different classes of subunit segregate (Supplementary Fig. 3).

Structural and model studies have suggested that a trimer of dimers acts as the nucleus in normal HBV capsid assembly[27,31,35]. Here, we showed that an artificially created hexamer can also function as nuclei to promote assembly. It suggests that capsid assembly can progress by various pathways that might arise from different types of nuclei. Manipulation of nuclei formation may change the course of assembly.

Resection of hybrid capsids to holey capsids. Previously, we attempted to generate holey capsids by removing modified subunits that had been incorporated stochastically; we were unable to identify regular, contiguous patches by this method[58]. However, our Janus capsids have a heterodimer hexamer patche in a body of crosslinked Cp150. We hypothesized that removing the heterodimer hexamers will leave Cp150

holey capsids intact due to their exceptional stability. To test this hypothesis, we purified hybrid capsids from a co-assembly reaction and removed heterodimer hexamers with a cocktail of 100 μM EDTA and 3 M urea. EDTA will disrupt the Ni^{2+} mediated interaction between His-Tags. Urea at 3 M weakens Cp-Cp interactions without unfolding dimer structures, allowing the heterodimer $Cp149_{His}Cp149_{Y132A}$ dimers to dissociate from the hybrid capsids[59]. We observed that EDTA and urea treatment decreased the amount of $Cp149_{His}$ associated with the presumably holey capsids based on SDS-PAGE and led to altered elution of capsid-sized particles on SEC (Supplementary Fig. 4a).

To validate the presence of holey capsids and not the selective dissociation of hexamer-enriched capsids, we analyzed purified holey capsids by resistive pulsive sensing (RPS)[46,60]. In RPS, solute displaces a proportional amount of electrolyte from a nanopore, resulting in a deflection of the current that is proportional to the volume of a single particle (Supplementary Fig. 5 and 6). It is a particularly powerful approach for working with low protein concentrations in the presence of non-volatile solutes. We found that EDTA and urea reduced the proportion of 120-dimer T=4 capsids, had little effect on the proportion of 90-dimer T=3 particles, and introduced a new heterogeneous mixture of incomplete, stable capsids (Fig. 4b, green line). The remaining T=4 and T=3 capsids may be assembled exclusively from Cp150 homodimers. This result confirmed that co-assembled $Cp149_{His}Cp149_{Y132A}$ hexamers can be removed, leaving potentially asymmetric holey capsids. Given that a 120-dimer capsid losing a single hexamer should have 114 dimers remaining, many capsids apparently had more than one hexamer or one double hexamer removed.

Cryo-EM reconstruction of holey capsids. To unambiguously confirm that asymmetric holey capsids had been created, we characterized the species in a resection reaction with cryo-EM. As predicted from our RPS results, raw micrographs of holey capsids showed a mixture of compete capsids and capsids with open edges (Fig. 5a, red arrows). 41,057 particles were selected and processed for 3D image reconstruction. Through the whole reconstruction process, C1 symmetry was applied to avoid losing unique features that would have been overwritten if we had used icosahedral symmetry averaging[61].

After 2D classification, the dataset was divided into two sets, one for complete capsids (23,478 particles) and the other for asymmetric holey capsids (17,579 particles). The dataset for complete capsids yielded a 6.2 Å resolution density map showing an apparently symmetrical 120-dimer capsid, though only C1 symmetry was applied (Fig 5b). We note that some capsids included in the complete capsid dataset may have had holes that were obscured by particle orientation. The holey capsid dataset was further divided into two sets by 3D classification, based on the size of the hole. In the end, 9,697 particles were used to reconstruct a 10.8 Å resolution density map for a holey capsid missing around a hexamer of dimers (Fig. 5c). The remaining 7,882 particles were reconstructed to yield a 12.9 Å resolution density map for a holey capsid missing approximately two hexamers (Fig. 5e). The two holey capsid density maps never reached the same resolution as the 120-dimer capsid density map. We believe that might be due to the use of fewer particles, particle heterogeneity, and potentially the greater flexibility of holey capsids.

To quantify the number of missing dimers on both reconstructions, we overlaid density maps for holey capsids at 1.3σ contour level on the density map for the120-dimer capsid density map. For the capsid with the smaller hole, density was missing for ~9 dimers centered around a hexamer (Fig. 5d). For the capsid with the bigger hole, ~18 dimers were missing from a hole that could be filled by a double hexamer and a pentamer (Fig. 5f). Initially, we suggested that during co-assembly, hexamers and double hexamers nucleated capsid formation. However, based on RPS there was no clear peak for holey capsids that lost exactly a hexamer or a double hexamer during capsid resection. Careful examination of both holey density maps showed degraded density close to edge of the hole, suggesting that particles used for reconstruction were not homogeneous. This heterogeneity could arise for multiple reasons: i) additional heterodimers could have associated with the built-in hexamer or the double hexamer during the co-assembly reaction, which would result in heterogeneity at edge of the hole, and ii) although the majority of the Cp150 homodimers crosslinked, dimers on the edge of the hole may not have crosslinked and were thus labile when exposed by resection. The heterogeneity of the holes observed by cryo-EM matches well with the apparent heterogeneity defined by RPS of holey capsids (Fig. 4b).

Holey capsids can be refilled to create asymmetric, un-holey capsids. Early attempts to characterize assembly pathways showed intermediates with sizes similar to holey capsid species that could proceed to assemble. However, we were unable to structurally characterize and isolate them, which may be due to their rarity and instability[56]. We reasoned that our holey capsids can also proceed to assemble to 120-dimer un-holey capsids, making them useful for containing cargo and for displaying surface features that were not part of the original nucleus or the capsid body. In effect, holey capsids are models of on-path assembly intermediates[56].

To test our ability to refill the holey capsids, we introduced a fluorescent homodimer, Cp150Bo, which has a BODIPY fluorophore attached to residue cysteine 150 of Cp150[48]. After the refilling reaction, using RPS, we observed that the amount of heterogenous holey capsids decreased nearly to the baseline and the amount of 120-dimer capsids, indistinguishable from control T=4 capsids, increased (Fig. 4b, blue line). This result indicated that holey capsids are assembly-active polymers to which Cp150Bo homodimers can be added. The appearance of bright fluorescence in chromatographic separations of un-holey capsids confirmed the addition of Cp150Bo (Fig. 4c, blue). For comparison, capsids of Cp150Bo alone are dimly fluorescent (Fig. 4c, orange), because BODIPY fluorophores are close to each other in the capsid interior, leading to fluorescence quenching[57]. In refilled holey capsids, there are no adjacent BIDIPY fluorophores on the edges of holes, leaving fluorophores unquenched. Thus, holey capsids can still react with free dimers, such as Cp150Bo. This result shows that other modified homodimers, potentially carrying novel moieties can be incorporated into the holey capsids through the refilling process. We suggest that with ligand targeting modifications, refilled capsids have potential for drug delivery to specific sites.

Conclusion

Symmetric subunits often spontaneously assemble into symmetric capsids with no stops[26,31]. Here, we showed a strategy to break the continuous HBV capsid assembly into a series of independent reactions. The key to this process is to design a heterodimer with distinct assembly properties programmed into each monomer. One monomer is assembly-active and can assemble in response to Ni^{2+}, whereas the other monomer is assembly-incompetent alone but can co-assemble with additional homodimers[34-36]. By manipulating assembly conditions with the novel designed heterodimer, a set of independent assembly reactions can be achieved. The different reactions yielded: hexamer, asymmetric co-assembled capsids, asymmetric holey capsids, and refilled asymmetric un-holey capsids. Formation of the asymmetric capsids mimics the assembly of bacteriophage P22 where a portal complex nucleates capsid assembly[62]. However, in this case, the “hexamer portals” can be removed to create asymmetric holey capsids that can be subsequently refilled with other engineered dimers. This reinvented process provides many opportunities to engineer asymmetric and symmetric capsids for applications[40,41], e.g., loading cargos into holey capsids, attaching a directing signal to refilling homodimers. We are effectively providing a path for making very small, 36-nm diameter, Janus particles with molecular uniformity. Though not every viral capsid is built from homodimers like HBV, many viral capsids have oligomeric subunits that could be asymmetrized[23-26]. We anticipate that our strategy to create an asymmetric assembly pathway and asymmetric capsids can be generalized to other viral capsids systems by redesigning the interaction interfaces from the same subunit. Asymmetric capsids from this process will open a window to create organized, multi-functionalized particles.

Declarations

Acknowledgements

We gratefully acknowledge support for this study from the NIH by R01 AI144022 to AZ and R01 GM129354 to SCJ. We gratefully acknowledge the use of the Laboratory for Biological Mass Spectrometry at Indiana University (IU) for the data in Fig 2c, the IU Electron Microscopy Center, and IU Nanoscale Characterization Facility. Electron microscopy at the IU Electron Microscopy Center was partially supported by a CTSI Spring 2019 grant to AZ.

References

1 Blundell, T. L. & Srinivasan, N. Symmetry, stability, and dynamics of multidomain and multicomponent protein systems. *Proc Natl Acad Sci U S A* **93**, 14243-14248, doi:10.1073/pnas.93.25.14243 (1996).

2 Levy, E. D., Boeri Erba, E., Robinson, C. V. & Teichmann, S. A. Assembly reflects evolution of protein complexes. *Nature* **453**, 1262-1265, doi:10.1038/nature06942 (2008).

3 Goodsell, D. S. & Olson, A. J. Structural symmetry and protein function. *Annu Rev Biophys Biomol Struct* **29**, 105-153, doi:10.1146/annurev.biophys.29.1.105 (2000).

4 Andre, I., Strauss, C. E., Kaplan, D. B., Bradley, P. & Baker, D. Emergence of symmetry in homooligomeric biological assemblies. *Proc Natl Acad Sci U S A* **105**, 16148-16152, doi:10.1073/pnas.0807576105 (2008).

5 Plaxco, K. W. & Gross, M. Protein complexes: the evolution of symmetry. *Curr Biol* **19**, R25-26, doi:10.1016/j.cub.2008.11.004 (2009).

6 Simon, A. J. *et al.* Supercharging enables organized assembly of synthetic biomolecules. *Nat Chem* **11**, 204-212, doi:10.1038/s41557-018-0196-3 (2019).

7 Kobayashi, N. & Arai, R. Design and construction of self-assembling supramolecular protein complexes using artificial and fusion proteins as nanoscale building blocks. *Curr Opin Biotechnol* **46**, 57-65, doi:10.1016/j.copbio.2017.01.001 (2017).

8 Butterfield, G. L. *et al.* Evolution of a designed protein assembly encapsulating its own RNA genome. *Nature* **552**, 415-420, doi:10.1038/nature25157 (2017).

9 King, N. P. *et al.* Computational design of self-assembling protein nanomaterials with atomic level accuracy. *Science* **336**, 1171-1174, doi:10.1126/science.1219364 (2012).

10 Yeates, T. O. Geometric Principles for Designing Highly Symmetric Self-Assembling Protein Nanomaterials. *Annu Rev Biophys* **46**, 23-42, doi:10.1146/annurev-biophys-070816-033928 (2017).

11 Alberstein, R., Suzuki, Y., Paesani, F. & Tezcan, F. A. Engineering the entropy-driven free-energy landscape of a dynamic nanoporous protein assembly. *Nat Chem* **10**, 732-739, doi:10.1038/s41557-018-0053-4 (2018).

12 Padilla, J. E., Colovos, C. & Yeates, T. O. Nanohedra: using symmetry to design self assembling protein cages, layers, crystals, and filaments. *Proc Natl Acad Sci U S A* **98**, 2217-2221, doi:10.1073/pnas.041614998 (2001).

13 Lai, Y. T., Cascio, D. & Yeates, T. O. Structure of a 16-nm cage designed by using protein oligomers. *Science* **336**, 1129, doi:10.1126/science.1219351 (2012).

14 Brodin, J. D., Carr, J. R., Sontz, P. A. & Tezcan, F. A. Exceptionally stable, redox-active supramolecular protein assemblies with emergent properties. *Proc Natl Acad Sci U S A* **111**, 2897-2902, doi:10.1073/pnas.1319866111 (2014).

15 Boyken, S. E. *et al.* De novo design of protein homo-oligomers with modular hydrogen-bond network-mediated specificity. *Science* **352**, 680-687, doi:10.1126/science.aad8865 (2016).

16 Huang, P. S., Boyken, S. E. & Baker, D. The coming of age of de novo protein design. *Nature* **537**, 320-327, doi:10.1038/nature19946 (2016).

17 Hsia, Y. *et al.* Design of a hyperstable 60-subunit protein dodecahedron. [corrected]. *Nature* **535**, 136-139, doi:10.1038/nature18010 (2016).

18 Douglas, T. & Young, M. Viruses: making friends with old foes. *Science* **312**, 873-875 (2006).

19 Douglas, T. & Young, M. Host-guest encapsulation of materials by assembled virus protein cages. *Nature* **393**, 152-155 (1998).

20 Steinmetz, N. F., Cho, C. F., Ablack, A., Lewis, J. D. & Manchester, M. Cowpea mosaic virus nanoparticles target surface vimentin on cancer cells. *Nanomedicine* **6**, 351-364, doi:10.2217/nnm.10.136 (2011).

21 Czapar, A. E. & Steinmetz, N. F. Plant viruses and bacteriophages for drug delivery in medicine and biotechnology. *Curr Opin Chem Biol* **38**, 108-116, doi:10.1016/j.cbpa.2017.03.013 (2017).

22 Lizotte, P. H. *et al.* In situ vaccination with cowpea mosaic virus nanoparticles suppresses metastatic cancer. *Nat Nanotechnol* **11**, 295-303, doi:10.1038/nnano.2015.292 (2016).

23 Wynne, S. A., Crowther, R. A. & Leslie, A. G. W. The crystal structure of the human hepatitis B virus capsid. *Mol Cell* **3**, 771-780, doi:Doi 10.1016/S1097-2765(01)80009-5 (1999).

24 Kang, S. *et al.* Implementation of p22 viral capsids as nanoplatforms. *Biomacromolecules* **11**, 2804-2809, doi:10.1021/bm100877q (2010).

25 Young, M., Willits, D., Uchida, M. & Douglas, T. Plant viruses as biotemplates for materials and their use in nanotechnology. *Annu Rev Phytopathol* **46**, 361-384 (2008).

26 Wen, A. M. & Steinmetz, N. F. Design of virus-based nanomaterials for medicine, biotechnology, and energy. *Chem Soc Rev* **45**, 4074-4126, doi:10.1039/c5cs00287g (2016).

27 Perlmutter, J. D. & Hagan, M. F. Mechanisms of virus assembly. *Annu Rev Phys Chem* **66**, 217-239, doi:10.1146/annurev-physchem-040214-121637 (2015).

28 Asor, R., Schlicksup, C. J., Zhao, Z., Zlotnick, A. & Raviv, U. Rapidly Forming Early Intermediate Structures Dictate the Pathway of Capsid Assembly. *J Am Chem Soc* **142**, 7868-7882,

doi:10.1021/jacs.0c01092 (2020).

29 Kler, S. *et al.* RNA encapsidation by SV40-derived nanoparticles follows a rapid two-state mechanism. *Journal of the American Chemical Society* **134**, 8823-8830, doi:10.1021/ja2110703 (2012).

30 Lutomski, C. A. *et al.* Hepatitis B Virus Capsid Completion Occurs through Error Correction. *J Am Chem Soc* **139**, 16932-16938, doi:10.1021/jacs.7b09932 (2017).

31 Zlotnick, A., Johnson, J. M., Wingfield, P. W., Stahl, S. J. & Endres, D. A theoretical model successfully identifies features of hepatitis B virus capsid assembly. *Biochemistry* **38**, 14644-14652 (1999).

32 Schlicksup, C. J. *et al.* Hepatitis B virus core protein allosteric modulators can distort and disrupt intact capsids. *Elife* **7**, doi:10.7554/eLife.31473 (2018).

33 Conway, J. F. *et al.* Visualization of a 4-helix bundle in the hepatitis B virus capsid by cryo-electron microscopy. *Nature* **386**, 91-94 (1997).

34 Zhao, Z. *et al.* Structural Differences between the Woodchuck Hepatitis Virus Core Protein in the Dimer and Capsid States Are Consistent with Entropic and Conformational Regulation of Assembly. *J Virol* **93**, doi:10.1128/JVI.00141-19 (2019).

35 Packianathan, C., Katen, S. P., Dann, C. E., 3rd & Zlotnick, A. Conformational changes in the hepatitis B virus core protein are consistent with a role for allostery in virus assembly. *J Virol* **84**, 1607-1615, doi:10.1128/JVI.02033-09 (2010).

36 Bourne, C. R., Katen, S. P., Fulz, M. R., Packianathan, C. & Zlotnick, A. A mutant hepatitis B virus core protein mimics inhibitors of icosahedral capsid self-assembly. *Biochemistry* **48**, 1736-1742, doi:10.1021/bi801814y (2009).

37 Damasceno, P. F., Engel, M. & Glotzer, S. C. Predictive self-assembly of polyhedra into complex structures. *Science* **337**, 453-457, doi:10.1126/science.1220869 (2012).

38 Paik, T. & Murray, C. B. Shape-directed binary assembly of anisotropic nanoplates: a nanocrystal puzzle with shape-complementary building blocks. *Nano Lett* **13**, 2952-2956, doi:10.1021/nl401370n (2013).

39 Zhang, Z. & Glotzer, S. C. Self-Assembly of Patchy Particles. *Nano Lett* **4**, 1407-1413, doi:10.1021/nl0493500 (2004).

40 Jiang, S. *et al.* Janus particle synthesis and assembly. *Advanced Materials* **22**, 1060-1071, doi:10.1002/adma.200904094 (2010).

41 Yan, J., Bloom, M., Bae, S. C., Luijten, E. & Granick, S. Linking synchronization to self-assembly using magnetic Janus colloids. *Nature* **491**, 578-581, doi:10.1038/nature11619 (2012).

42 Zhao, Z., Wang, J. C., Segura, C. P., Hadden-Perilla, J. A. & Zlotnick, A. The integrity of the intradimer interface of the Hepatitis B Virus capsid protein dimer regulates capsid self-assembly. *ACS Chem Biol*, doi:10.1021/acschembio.0c00277 (2020).

43 Contino, N. C. & Jarrold, M. F. Charge detection mass spectrometry for single ions with a limit of detection of 30 charges. *Int. J. Mass Spect.* **345–347**, 153–159 (2013).

44 Harms, Z. D., Selzer, L., Zlotnick, A. & Jacobson, S. C. Monitoring Assembly of Virus Capsids with Nanofluidic Devices. *ACS Nano* **9**, 9087-9096, doi:10.1021/acsnano.5b03231 (2015).

45 Kondylis, P. *et al.* Evolution of Intermediates during Capsid Assembly of Hepatitis B Virus with Phenylpropenamide-Based Antivirals. *Acs Infectious Diseases* **5**, 769-777, doi:10.1021/acsinfecdis.8b00290 (2019).

46 Zhou, J. *et al.* Characterization of Virus Capsids and Their Assembly Intermediates by Multicycle Resistive-Pulse Sensing with Four Pores in Series. *Anal Chem* **90**, 7267-7274, doi:10.1021/acs.analchem.8b00452 (2018).

47 Hengen, P. Purification of His-Tag fusion proteins from Escherichia coli. *Trends Biochem Sci* **20**, 285-286, doi:10.1016/s0968-0004(00)89045-3 (1995).

48 Stray, S. J., Johnson, J. M., Kopek, B. G. & Zlotnick, A. An in vitro fluorescence screen to identify antivirals that disrupt hepatitis B virus capsid assembly. *Nat Biotechnol* **24**, 358-362, doi:10.1038/nbt1187 (2006).

49 Zlotnick, A. *et al.* In vitro screening for molecules that affect virus capsid assembly (and other protein association reactions). *Nature Protocols* **2**, 490-498 (2007).

50 Walker, A., Skamel, C. & Nassal, M. SplitCore: an exceptionally versatile viral nanoparticle for native whole protein display regardless of 3D structure. *Sci Rep* **1**, 5, doi:10.1038/srep00005 (2011).

51 Pumpens, P. & Grens, E. HBV core particles as a carrier for B cell/T cell epitopes. *Intervirology* **44**, 98-114, doi:10.1159/000050037 (2001).

52 Schodel, F. *et al.* The position of heterologous epitopes inserted in hepatitis B virus core particles determines their immunogenicity. *J Virol* **66**, 106-114 (1992).

53 Kratz, P. A., Bottcher, B. & Nassal, M. Native display of complete foreign protein domains on the surface of hepatitis B virus capsids. *Proc Natl Acad Sci U S A* **96**, 1915-1920 (1999).

54 Peyret, H. *et al.* Tandem fusion of hepatitis B core antigen allows assembly of virus-like particles in bacteria and plants with enhanced capacity to accommodate foreign proteins. *PLoS One* **10**, e0120751, doi:10.1371/journal.pone.0120751 (2015).

55 Holmes, K. *et al.* Assembly Pathway of Hepatitis B Core Virus-like Particles from Genetically Fused Dimers. *J Biol Chem* **290**, 16238-16245, doi:10.1074/jbc.M114.622035 (2015).

56 Pierson, E. E. *et al.* Detection of late intermediates in virus capsid assembly by charge detection mass spectrometry. *J Am Chem Soc* **136**, 3536-3541, doi:10.1021/ja411460w (2014).

57 Shreffler, W. G., Lencer, D. A., Bardina, L. & Sampson, H. A. IgE and IgG4 epitope mapping by microarray immunoassay reveals the diversity of immune response to the peanut allergen, Ara h 2. *J Allergy Clin Immunol* **116**, 893-899, doi:10.1016/j.jaci.2005.06.033 (2005).

58 Lee, L. S. *et al.* A Molecular Breadboard: Removal and Replacement of Subunits in an Hepatitis B Virus Capsid *in progress* (2017).

59 Singh, S. & Zlotnick, A. Observed hysteresis of virus capsid disassembly is implicit in kinetic models of assembly. *J Biol Chem* **278**, 18249-18255, doi:10.1074/jbc.M211408200 (2003).

60 Kondylis, P., Schlicksup, C. J., Zlotnick, A. & Jacobson, S. C. Analytical Techniques to Characterize the Structure, Properties, and Assembly of Virus Capsids. *Anal Chem*, doi:10.1021/acs.analchem.8b04824 (2018).

61 Wang, J. C., Mukhopadhyay, S. & Zlotnick, A. Geometric Defects and Icosahedral Viruses. *Viruses* **10**, pii: E25, doi:10.3390/v10010025 (2018).

62 Motwani, T. & Teschke, C. M. Architect of Virus Assembly: the Portal Protein Nucleates Procapsid Assembly in Bacteriophage P22. *Journal of virology* **93**, doi:10.1128/JVI.00187-19 (2019).

Figures

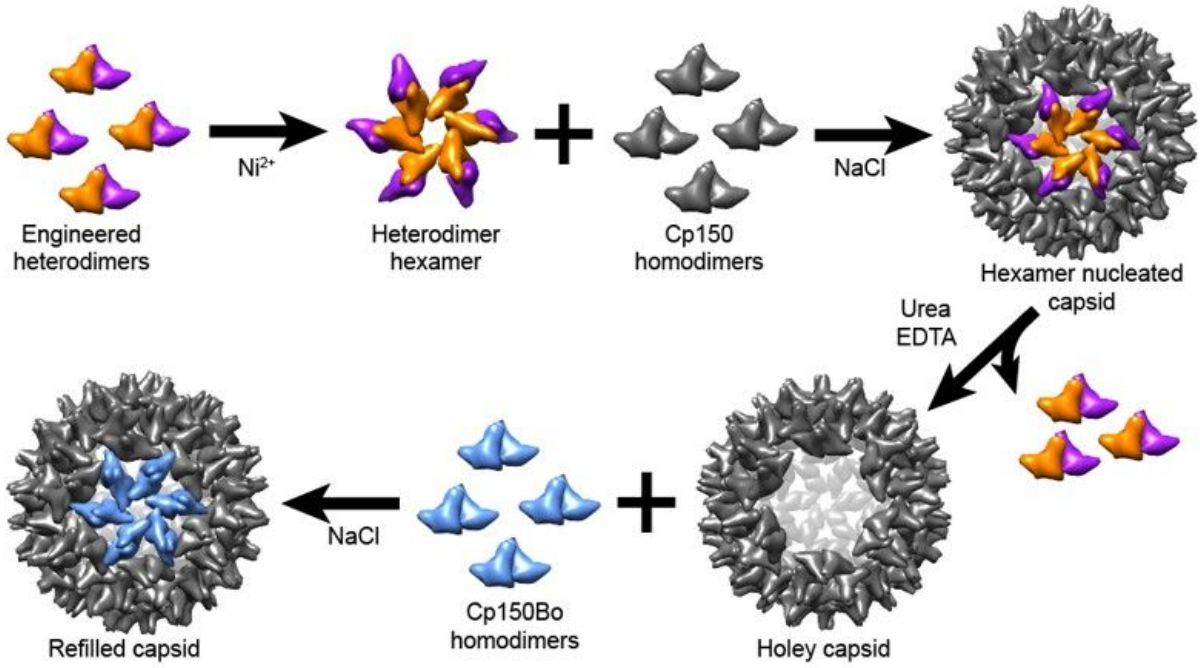

Figure 1

Schematic of the hierarchical assembly of an HBV capsid analog starting with an asymmetric dimeric subunit. Engineered HBV heterodimers assemble into hexamers by addition of Ni2+. The hexamer model in this figure provides a low-resolution representation of the interaction between dimers. Hexamers nucleate co-assembly with homodimers into capsids. Co-assembled capsids are disassembled into holey capsids by removing the hexameric nucleus. Holey capsids then can be refilled into compete capsids with addition of a new species of homodimer. Note that the co-assembled capsid and refilled capsid have a defined patch, allowing display of a unique surface chemistry. Also, the opening in the holey capsid offers the opportunity to add a novel cargo to the capsid.

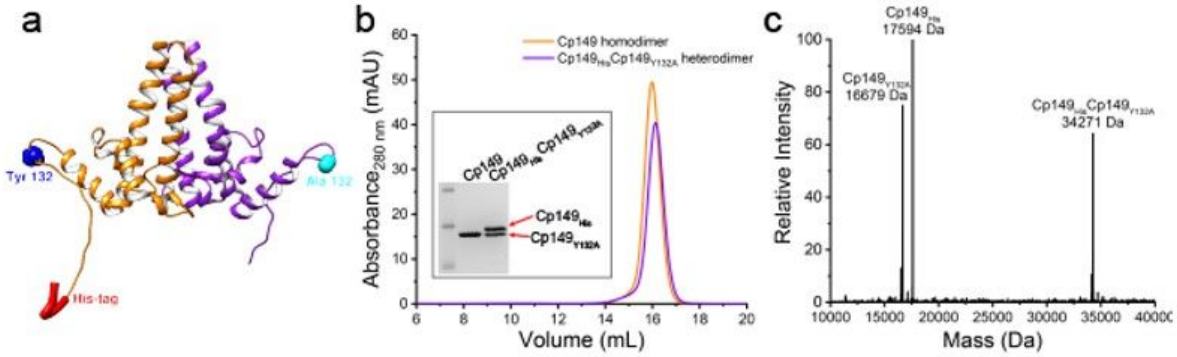

Figure 2

Design and purification of the engineered heterodimer, Cp149HisCp149Y132A. a, A model of the modified heterodimer based on 1QGT. The contact helix and subsequent loops, with residue 132, extend to the right and left of the base of the dimer. A 6 histidine His-Tag is attached to the C-terminus of one monomer (orange), and an assembly incompetent mutation (Y132A) is present on the other monomer (purple). b, Purified heterodimer, Cp149HisCp149Y132A, shows a single peak by SEC and elutes similarly to purified Cp149 homodimers. SDS-PAGE shows a single band for Cp149 homodimers, whereas Cp149HisCp149Y132A shows two equally dense bands corresponding to the two different monomers (inset). c, Native mass spectrometry of Cp149HisCp149Y132A shows three species corresponding to the different monomers and the disulfide crosslinked heterodimer. No MS evidence was found for the Cp149¬¬His homodimer or Cp149Y132A homodimer.

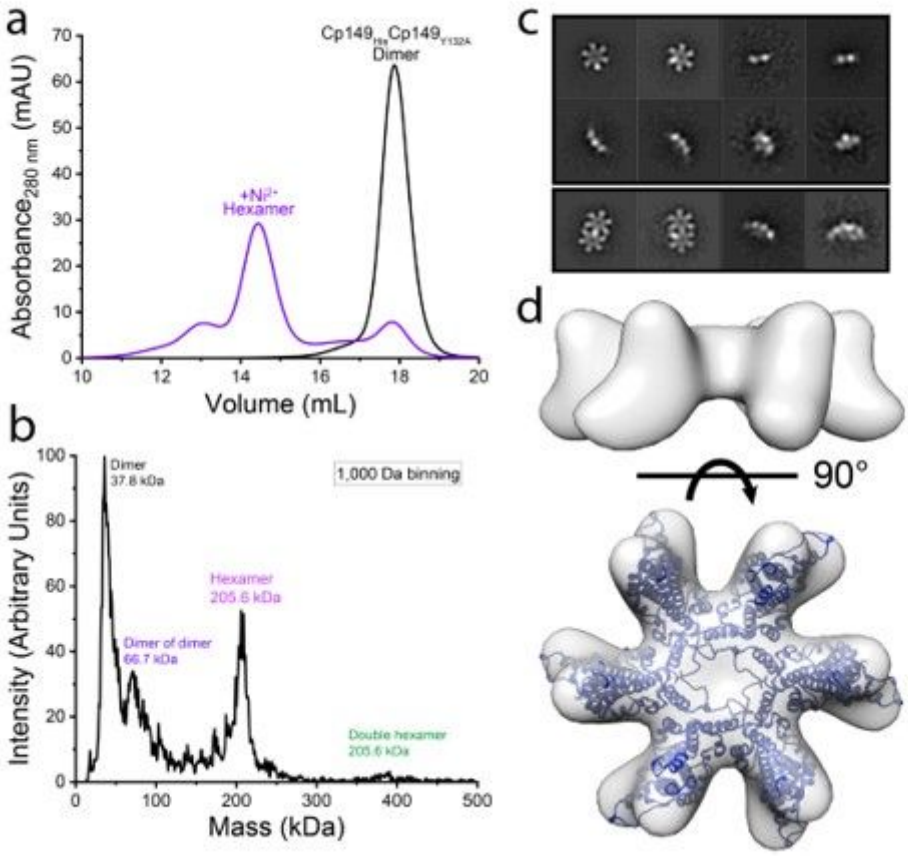

Figure 3

Characterization of heterodimer hexamers. a, SEC shows that with the addition of Ni2+, Cp149HisCp149Y132A heterodimers form larger species and elute earlier than heterodimers. b, CDMS demonstrates that Ni2+ induces formation of hexamers. c, Class average of negative stain EM of purified hexamers shows top and side views of hexamers. Double hexamers are also observed. d, A 17 Å resolution hexamer density map reconstructed from negative stain EM (side and top views) matches well with a hexamer model isolated from an HBV capsid (1QGT).

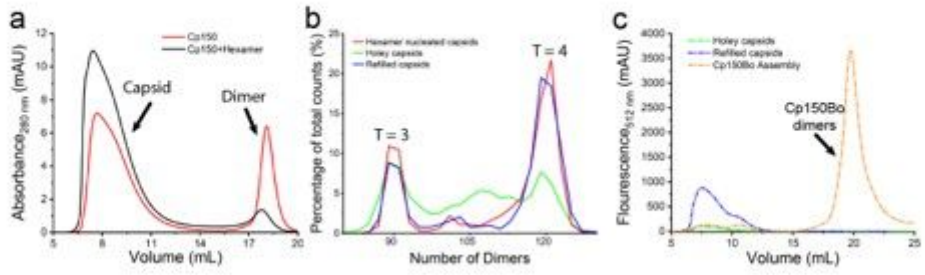

Figure 4

Generating holey capsids through co-assembly and disassembly and refilling holey capsids. a, SEC shows that heterodimer hexamers co-assemble with Cp150 homodimers (black) to generate more capsids than Cp150 homodimer itself (red). b, RPS analysis of co-assembled capsids, holey capsids, and refilled capsids. Purified co-assembled capsids have two major species, T=3 and T=4 capsids (red line). After the disassembly process, holey capsids are generated from T=4 capsids resulting in a heterogenous array of incomplete holey capsids (green line). With addition of Cp150Bo homodimer, holey capsids are refilled back to T=4 capsids (blue line). c, SEC with a fluorescence detector shows that Cp150Bo co-elute with refilled capsids.

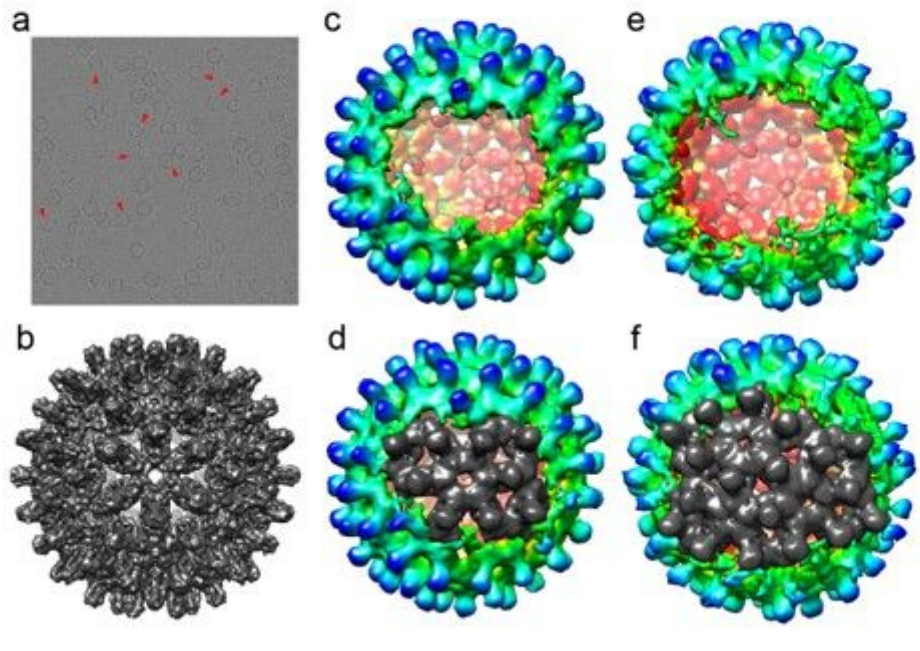

Figure 5

Cryo-EM characterization of holey capsids. a, A cryo-EM micrograph of a holey capsid sample. Several obvious holey capsids are pointed out by red arrows. b, c and e, Reconstructions yielded a 120-dimer

complete capsid (b) and two species of holey capsids (c and e). d and f, Comparing holey to complete capsid maps shows that the capsid with the small hole (c and d) is missing density for 9 dimers including one hexamer. Whereas the capsid with a bigger hole (e and f) is missing density for ~18 dimers including two hexamers and a pentamer. The partial subunits at the periphery of the holes suggests heterogeneity of hole size and mobility of peripheral dimers. For these figures, capsid density is contoured at 1.3 Å. Holey capsids are colored by radius.

Supplementary Files

This is a list of supplementary files associated with this preprint. Click to download.

- 20200615supportinginformation.docx